ISSN 0023-1584, Kinetics and Catalysis, 2009, Vol. 50, No. 1, pp. 40–47. © Pleiades Publishing, Ltd., 2009.
Original Russian Text © V.I. Elokhin, A.V. Matveev, V.V. Gorodetskii, 2009, published in Kinetika i Kataliz, 2009, Vol. 50, No. 1, pp. 46–53.

FIFTY YEARS
OF THE BORESKOV INSTITUTE OF CATALYSIS

Self-Oscillations and Chemical Waves in CO Oxidation on Pt and Pd: Kinetic Monte Carlo Models

V. I. Elokhin[a,b], A. V. Matveev[a,b], and V. V. Gorodetskii[a]

[a] *Boreskov Institute of Catalysis, Siberian Branch, Russian Academy of Sciences, Novosibirsk, 630090 Russia*
[b] *Novosibirsk State University, Novosibirsk, 630090 Russia*
e-mail:elokhin@catalysis.ru

Received April 18, 2008

Abstract—Theoretical studies of the spatiotemporal dynamics of CO oxidation on Pt(100) and Pd(110) single crystal surfaces have been carried out by the kinetic Monte Carlo method. For both surfaces, Monte Carlo simulation has revealed oscillations of the CO_2 formation rate and of the concentrations of adsorbed species. The oscillations are accompanied by wave processes on the model surface. Simulations have demonstrated that there is a narrow reaction zone when an oxygen wave propagates over the surface. The existence of this zone has been confirmed by experimental studies. Taking into account the anisotropy of the Pd(110) crystal has no effect on the oscillation period and amplitude, but leads to the formation of elliptic oxygen patterns on the surface. It is possible to obtain a wide variety of chemical waves (cellular and turbulent structures, spirals, rings, and strips) by varying the parameters of the computational experiment.

DOI: 10.1134/S0023158409010066

Catalytic CO oxidation on platinum-group metals is a classical model reaction in heterogeneous catalysis. In addition to being of fundamental interest, this reaction is of great environmental significance as a means of removing carbon monoxide from exhaust gases. CO oxidation under far-from-equilibrium conditions can be accompanied by critical phenomena, such as multiple steady states, self-oscillations, traveling waves, and chaos [1–15]. Various autooscillation mechanisms have been discovered and investigated to date. These include surface phase transitions [4, 6], the formation of a "subsurface" oxygen layer [12], and the "explosive" interaction between adsorbed species [14]. For all of the mechanisms, it is assumed that the metal surface passes spontaneously and periodically from the inactive state to the highly catalytic active state.

Use of physical methods with a high space resolution (<1 μm) made it possible to study in situ the formation of traveling chemical waves arising from the oscillatory dynamics of the reaction on Pt and Pd single-crystal surfaces [11, 13]. It was demonstrated that the conventional approaches using phenomenological kinetic equations (sets of differential equations) are inappropriate for describing the nature of spatiotemporal chemical waves on the metal surface [16]. So-called kinetic (dynamic) Monte Carlo models [17] turned out to be the most suitable. The most recent review of the application of these models to oscillatory reactions was given by Zhdanov [18]. Here, we present an overview of our recent experimental and theoretical Monte Carlo studies of the mechanism of the formation of self-oscillations and chemical waves in CO oxidation on Pt(100) and Pd(110) single crystals.

MODELS

Pt(100): Simulation of Self-Oscillations and Chemical Waves

The detailed reaction mechanism used in the simulation of the self-oscillations [19–22] is based on experimental data reported in [23–36]. It was discovered that the self-oscillations of the CO oxidation rate are related with the reversible phase transition Pt(100)-(*hex*) $\longleftrightarrow$ (1×1).

Ertl's model distinguishes the following stages of the self-oscillation cycle in CO oxidation on the Pt(100) surface [4, 11]:

(1) When the reaction medium ($P_{CO}/P_{O_2} \approx 1 : 10$) is in contact with the clean reconstructed surface (*hex*), because of the smallness of the oxygen sticking coefficient ($s_{O_2} \approx 10^{-3}$), CO adsorption ($s_{CO} \approx 0.8$) mainly takes place. Once a surface coverage of $\theta_{CO} \approx 0.08$ is reached, the phase transition (*hex*) $\longrightarrow$ (1×1) occurs rapidly, resulting in the formation and growth of (1×1) islands over the surface.

(2) The appearance of the nonreconstructed surface (1×1) causes a sharp increase in the oxygen adsorption rate ($s_{O_2} \approx 10^{-1}$ on (1×1)) and leads to complete coverage of the surface with an O_{ads} layer. The rapid reaction between CO_{ads} and O_{ads} on the (1×1) surface, which

increases the number of empty sites for the dissociative adsorption of O_2, initiates the autocatalytic formation of CO_2 molecules.

(3) The appearance of the clean (1×1) surface, which is thermodynamically unstable under the reaction conditions, brings about a spontaneous back transition to reconstructed Pt(100)-*hex*, and the oscillation cycle is thus completed.

The mechanism of the reaction can be represented as

$$\mathrm{CO} + * \longrightarrow \mathrm{CO}_{\mathrm{ads}}, \quad \text{(I)}$$

$$\mathrm{CO}_{\mathrm{ads}}^{hex} \longrightarrow \mathrm{CO} + *_{hex}, \quad \text{(II)}$$

$$\mathrm{CO}_{\mathrm{ads}}^{1\times1} \longrightarrow \mathrm{CO} + *_{1\times1}, \quad \text{(III)}$$

$$(hex) \longrightarrow (1\times1)\text{: } 4\mathrm{CO}_{\mathrm{ads}} \longrightarrow 4\mathrm{CO}_{\mathrm{ads}}^{1\times1}, \quad \text{(IV)}$$

$$(1\times1) \longrightarrow (hex)\text{: } *_{1\times1} \longrightarrow *_{hex}, \quad \text{(V)}$$

$$\mathrm{O}_2 + 2*_{1\times1} \longrightarrow 2\mathrm{O}_{\mathrm{ads}}^{1\times1}, \quad \text{(VI)}$$

$$\mathrm{O}_{\mathrm{ads}}^{1\times1} + \mathrm{CO}_{\mathrm{ads}} \longrightarrow \mathrm{CO}_2 + *_{1\times1} + *, \quad \text{(VII)}$$

$$\mathrm{CO}_{\mathrm{ads}} + * \longrightarrow * + \mathrm{CO}_{\mathrm{ads}}. \quad \text{(VIII)}$$

Scheme 1.

Below, we present a brief description of the steps of this catalytic cycle. Step (I) is CO adsorption. The absence of indices at the active site * means that CO, unlike oxygen, has the same sticking coefficient (s_{CO}) for $*_{hex}$ and $*_{1\times1}$. Steps (II) and (III) are CO desorption. The rate constants of CO desorption from the surface phases (*hex*) and (1×1) differ by approximately 3–4 orders of magnitude. Step (IV) is the (*hex*) $\longrightarrow$ (1×1) phase transition. In accordance with [30, 35], it is assumed that only CO molecules adsorbed simultaneously on the four nearest neighbor sites of the model grid can cause its transformation into the (1×1) structure (with some probability). Step (V) is the back structural transition $(1\times1) \longrightarrow$ (*hex*). Step (VI) is oxygen adsorption. The dissociative adsorption of O_2 takes place only on double nearest neighbor (1×1)-type sites. Step (VII) is CO_2 formation. This reaction occurs via the Langmuir–Hinshelwood mechanism. O_{ads} reacts with CO_{ads}^{hex} and $CO_{ads}^{1\times1}$ at equal rates, and the kinds of active sites remain unchanged. Step (VIII) is CO_{ads} diffusion. The adsorbed molecule CO_{ads} diffuses on the surface by hopping from its site to a random nearest neighbor empty site. As this takes place, the kinds of active sites remain unchanged. Along with steps (III) and (VII), diffusion (VIII) is a source of empty $*_{1\times1}$ active sites, which are necessary for the dissociative adsorption of oxygen.

CO oxidation on Pt(100) was simulated on an $N \times N$ grid of square cells with cyclic boundary conditions (usually, we took $N = 1000$). The state of a cell was set according to the rules determined by the detailed reaction mechanism. The time unit was a Monte Carlo (MC) step, which consisted of $N \times N$ choice and realization trials of the main elementary processes. The probability of occurrence of each step for the adsorption, desorption, and chemical reaction processes was taken to be equal to the ratio of the rate constant of this step to the sum of the rate constants of all steps. The rate constants of steps (I)–(VII) at $T \sim 500$ K were taken from [27, Table 1].

After selecting one of the processes (steps (I)–(VII)) and performing a realization trial, we considered the internal cycle of diffusion, which consisted of M diffusion trials for CO_{ads} molecules (typically, $M = 50$–100). The CO oxidation rate and the reactant coverages of the surface were calculated after each MC step as the number of the resulting CO_2 molecules (or the number of cells in the corresponding state) divided by the total number of cells, N^2. The algorithm of the simulation of CO oxidation on Pt(100) is detailed elsewhere [19].

The Monte Carlo model of the reaction reveals oscillations of the reaction rate and the CO_{ads} and O_{ads} coverages of the surface and intertransitions between the surface phases (1×1) and (*hex*) under conditions similar to experimental results (the rate constants of the reaction steps were taken from [27]). The oscillations are accompanied by the propagation of concentration waves on the surface (Fig. 1). The most noteworthy result of the simulation is the revealing of a narrow reaction zone before the front of the propagating oxygen wave, which suggests that the surface passes into a highly active catalytic state (Fig. 2). It can be seen from Fig. 2 that the local CO_2 formation rate is the lowest in the CO_{ads} layer, takes an intermediate value in the O_{ads} layer, and is the highest in the narrow reaction zone along the perimeter of the growing O_{ads} islands. Note that this narrow reaction zone is observed only when there is a propagating oxygen wave. A local increase in the CO_{ads} concentration on the surface causes the disappearance of the narrow reaction zone, as follows from the behavior of an oxygen island (A) in the bottom left corner of Fig. 1. This island disappears as its oxygen reacts with CO_{ads}. Here, as O_{ads} is consumed, the vacated (1×1) phase turns into (*hex*). The observed difference between the local reaction rates can be

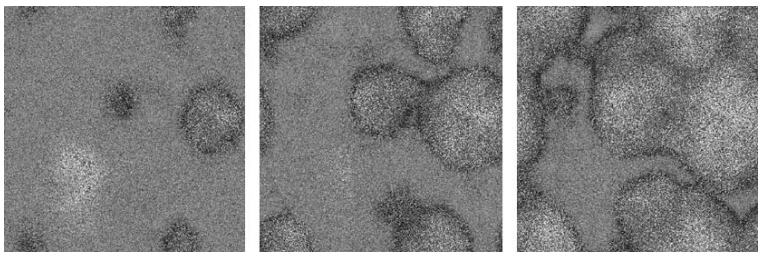

Fig. 1. Computer film frames depicting the propagation of an oxygen wave at the reaction rate increase stage. The light areas are O_{ads}, the dark areas are CO_{ads}, and the black areas are empty surface sites. The interframe time interval is 10 MC steps. The grid size is 1000×1000 cells. The CO_{ads} diffusion rate parameter is $M = 100$. Reaction conditions: $T \sim 500$ K, $P_{CO} = 5 \times 10^{-5}$ Torr, and $P_{O_2} = 7.5 \times 10^{-5}$ Torr. For rate constant data, see [19, 27].

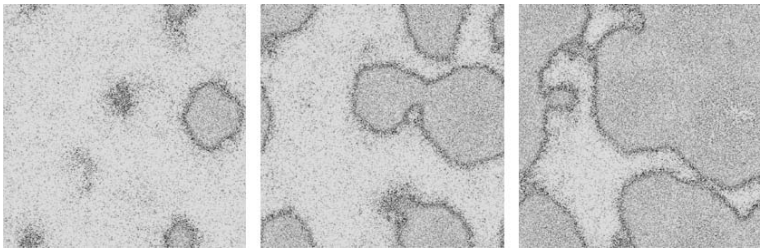

Fig. 2. Computer film frames depicting the variation of the CO_2 formation rate during the propagation of oxygen waves over the Pt(100) surface (see Fig. 1). The intensification of gray color means an increase in the CO_2 formation rate.

explained in terms of competitive oxygen and carbon monoxide adsorption: the CO_{ads} layer inhibits the dissociative adsorption of oxygen, while the O_{ads} layer always has single vacant sites for monomolecular CO adsorption. The highest total reaction rate in an oscillation period is reached at the instant the perimeter of the growing oxygen islands is the longest. At the final stage of the autooscillation cycle, the (1×1) phase turns into (*hex*) and the CO_{ads} coverage increases owing to CO adsorption on empty sites (both on (*hex*) and (1×1)). The appearance of a narrow reaction zone during oxygen wave propagation was observed experimentally in H_2 and CO oxidation on a Pt[100] oriented tip by atom-probe field ion microscopy (APFIM) with a resolution of ~5 Å [37, 38] (the experimental setup is schematized in Fig. 3).

Obviously, in order to synchronize the spatiotemporal changes in different areas of the surface, it is necessary to take into account the diffusion of the adsorbed species. However, the inclusion of diffusion into the set of randomly chosen main processes (in our case, steps (I)–(VII)) leads to an unreasonable lengthening of the computational time because the diffusion rate constant is several orders of magnitude larger than the rate constants of the other processes. For this reason, most researchers employing kinetic Monte Carlo models in which diffusion must be taken into account consider an internal diffusion cycle, making M random transfer trials for the adsorbed substances (in our case, only CO_{ads}). Since an increase in the diffusion cycle parameter M above 100 does not result in quantitative or qualitative changes in the spatiotemporal dynamics of the reaction, we believe that the chosen value of the CO_{ads} diffusion rate parameter is sufficiently large for synchronization of the local processes. Likewise, decreasing the parameter M to 50 does not break the regularity of the oscillations, but somewhat reduces the oscillation period and amplitude. A further decrease in M to 20 randomizes the oscillation period and amplitude. In this case, adsorbed oxygen is always present on the surface as mobile patches of various shapes (Fig. 4). A similar turbulent spatiotemporal dynamics of substances adsorbed on the Pt(100) surface in CO oxidation was observed by photoelectron emission microscopy (PEEM) [39] and by ellipsomicroscopy for surface imaging (EMSI) [40].

The kinetic Monte Carlo method provides a means to study the dependence of oscillation characteristics on reaction parameters. This can be done by varying some reaction parameter (e.g., CO partial pressure) from one step to another and using the surface coverage configuration calculated in the previous step as the initial condition for the next step. In this way, we found that a reaction rate and surface coverage hysteresis takes place as P_{CO} is first raised and then decreased in the 10^{-5}–1.2×10^{-4} Torr range at a fixed oxygen partial

pressure of $P_{O_2} = 2 \times 10^{-4}$ Torr [19]. At a higher P_{O_2}/P_{CO} ratio, the Pt(100)-*hex* surface is almost free. As P_{CO} is raised, the $CO_{ads}(1 \times 1)$ phase appears. At $P_{CO} \sim 3 \times 10^{-5}$ Torr, oscillations set in, whose amplitude and period increase with increasing P_{CO}. At $P_{CO} \sim 10^{-4}$ Torr, the surface is completely covered by a $CO_{ads}(1 \times 1)$ layer. As P_{CO} is then decreased, the $CO_{ads}(1 \times 1)$ layer persists down to $P_{CO} \sim 5 \times 10^{-6}$ Torr because of the low probability of CO desorption. Therefore, it is the $CO_{ads}(1 \times 1)$ desorption constant that determined the lower limit of the hysteresis. The back transition $(1 \times 1) \longrightarrow$ (*hex*) occurs vary rapidly (clean-off reaction [22]) via steps (V)–(VII).

Pd(110): Simulation of Oscillations and Wave Structures

As distinct from the oscillations on the Pt(100) surface, which are caused by surface phase transformation, the oscillations and wave phenomena on the Pd(110) surface are due to merely kinetic factors, specifically, changes in the catalytic and adsorption properties of the surface, including the oxygen sticking coefficient, because of the comparatively slow formation and consumption of subsurface oxygen, $O_{ads} \longleftrightarrow O_{sub}$. The adsorption and catalytic properties of Pd(110) were studied by various kinetic and physical methods [41–51]. A reaction mechanism taking into account the formation of subsurface oxygen O_{sub} [52] was suggested to explain the observed oscillations of the CO oxidation rate on Pt, Pd, and Ir [53–55]. It is assumed in this mechanism that the resulting O_{sub} layer suppresses oxygen adsorption and favors the growth of a CO_{ads} layer (inactive surface) [52]. Nevertheless, the slow reaction between CO_{ads} and O_{sub} removes subsurface oxygen, thus making oxygen adsorption a more favorable process (active surface). This causes O_{sub} formation again, so the cycle is repeated.

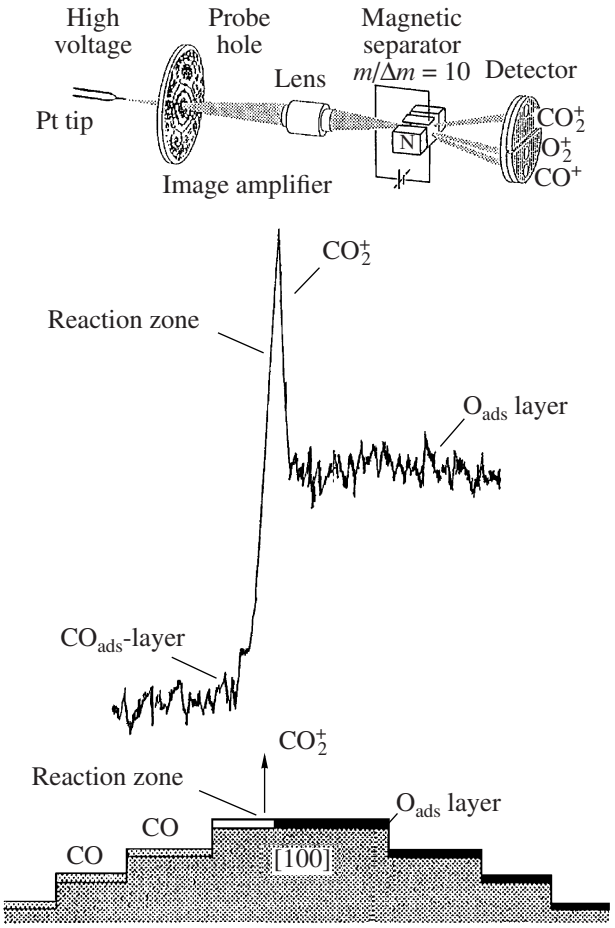

Fig. 3. Field ion microscopy setup for detecting the narrow reaction zone in CO oxidation on a platinum tip [38]. The preadsorbed CO_{ads} layer reacts with oxygen to form a narrow wave front crossing the probe hole in ~100 ms.

Based on experimental data, we formulated the following detailed mechanism of CO oxidation on Pd(110), which was then used in the kinetic simulation of this reaction by the Monte Carlo method [56]:

$$(1)\ O_{2(gas)} + 2* \longrightarrow 2O_{ads}, \qquad (4)\ O_{ads} + *_v \longrightarrow *O_{sub},$$

$$(2)\ CO_{(gas)} + * \longleftrightarrow CO_{ads}, \qquad (5)\ CO_{ads} + *O_{sub} \longrightarrow CO_{2(gas)} + 2* + *_v,$$

$$(3)\ CO_{ads} + O_{ads} \longrightarrow CO_{2(gas)} + 2*, \qquad (6)\ CO_{(gas)} + *O_{sub} \longleftrightarrow CO_{ads}O_{sub},$$

$$(7)\ CO_{ads}O_{sub} \longrightarrow CO_{2(gas)} + * + *_v.$$

Scheme 2.

Here, $*$ and $*_v$ are active sites of the surface and of the subsurface layer. The first step is irreversible oxygen adsorption, and the second is CO adsorption and desorption. In the third step, CO_{ads} reacts with O_{ads} to yield the reaction product. Subsurface oxygen, O_{sub}, forms in the irreversible step (4). Step (5) is the slow reaction between O_{sub} and the nearest neighbor CO_{ads} molecules, which regenerates the initial active sites of the surface, $*$. The adsorbed species $CO_{ads}O_{sub}$ results both from CO adsorption from the gas phase (step (6)) and from CO_{ads} diffusion over active sites, both initial and modified (O_{sub}). The decomposition of the $CO_{ads}O_{sub}$ complex yields CO_2 and vacates the $*$ and $*_v$ sites (step (7)). It is assumed that the heat of CO adsorption is lower on the modified sites O_{sub} than on the initial sites *; that is, the probability of $CO_{ads}O_{sub}$ desorp-

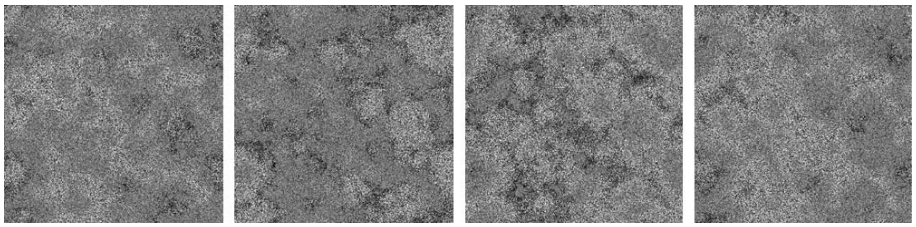

Fig. 4. Computer film frames depicting the variation of the oxygen concentration during an oscillation period of the reaction rate. The light areas are O_{ads}, the dark areas are CO_{ads}, and the black areas are empty surface sites. The interframe time interval is 20 MC steps. The grid size is 1000×1000 cells. The CO_{ads} diffusion rate parameter is $M = 20$. Reaction conditions: $T \sim 500$ K, $P_{CO} = 5 \times 10^{-5}$ Torr, and $P_{O_2} = 7.5 \times 10^{-5}$ Torr. For rate constant data, see [19, 27].

tion (step (6)) is higher than the probability of CO_{ads} desorption (step (2)). CO_{ads} can diffuse over the surface, obeying the following formal rules: 1. $CO_{ads} + * \longleftrightarrow * + CO_{ads}$, 2. $CO_{ads} + *O_{sub} \longleftrightarrow * + CO_{ads}O_{sub}$, and 3. $CO_{ads}O_{sub} + *O_{sub} \longleftrightarrow *O_{sub} + CO_{ads}O_{sub}$. The sequence of steps (1)–(5) [52] has frequently been used in the simulation of oscillations in catalytic oxidation reactions using either differential equations (see earlier reviews [7, 18]) or kinetic Monte Carlo methods [18], including in our studies [57–59]. In our earlier work [56], as well as in later studies [20–22, 60–63], the conventional steps (1)–(5) in Scheme 2 were supplemented with the possible formation and consumption of the surface species $CO_{ads}O_{sub}$ (steps (6) and (7)). Note that steps (6) and (7) diminish the range of existence of oscillations in the (T, P_i) space.

The Pd(110) surface was modeled as an $N \times N$ square grid (in our calculations, N = 500–8000) with square cells and cyclic (sometimes, zero) boundary conditions. For Pd(110), a cell can assume one of five states (*, CO_{ads}, O_{ads}, [$*O_{sub}$], [$CO_{ads}O_{sub}$]) according to the rules given by the algorithm of the simulation of the detailed reaction mechanism (Scheme 2). Here, the simulation algorithms are the same as were used in the simulation of CO oxidation dynamics on Pt(100) [56, 60–62].

The oscillatory behavior of CO oxidation on Pd(110), which takes place via the detailed mechanism presented in Scheme 2, was revealed by computational experiments [56] using the following set of rate constants of the elementary steps (s^{-1}):

k_1	k_2	k_{-2}	k_4	k_5	k_6	k_{-6}	k_7
1	1	0.2	0.03	0.01	1	0.5	0.02

The oscillations are accompanied by the wavelike propagation of adsorbed species over the surface. A dramatic increase in the reaction rate takes place at the minimum O_{sub} concentration value within one oscillation period simultaneously with the removal of the CO_{ads} layer and with the coverage of the surface by adsorbed oxygen (Fig. 5). Once the maximum reaction rate is achieved, a redistribution of adsorbed oxygen occurs: $O_{ads} \longrightarrow O_{sub}$. The position of the $O_{sub}(t)$ peak determines the point at which the reaction rate begins to decrease. CO_{ads} accumulates on the surface, and this is accompanied by the removal of the O_{ads} layer. When the reaction rate is the lowest, the CO_{ads} molecules react slowly with O_{sub}. A decrease in the O_{sub} concentration to some critical values recreates the conditions necessary for subsequent O_{ads} adsorption, so the self-oscillation cycle is repeated. As the oxygen wave front propagates, there is a narrow reaction zone with an increased concentration of empty active sites and a local maximum of the CO_2 formation rate.

Oxygen or CO adsorption on Pd(110) (Scheme 2, steps (1) and (2)) causes surface reconstruction into a so-called added/missing row structure, Pd(110)-$(1 \times 1) \longrightarrow (1 \times 2)$, and this is not accompanied by any significant change in the adsorption or catalytic properties of the surface. Surface anisotropy is observed here: CO_{ads} molecules diffuse more rapidly along metal atom rows than in the transverse direction. We demonstrated that, if this effect is taken into account in the Monte Carlo model of the reaction [61], then varying the M_x/M_y ratio (M_x is the number of CO_{ads} diffusion trials in the direction x, which coincides with the direction $[1\bar{1}0]$ on the Pd(110)-(1×2) surface, and M_y is the number of CO_{ads} diffusion trials in the direction y, with the total diffusion rate in the internal cycle remaining invariable: $M_x + M_y = M$) will not change the dependences of the reaction rate and adsorbed species coverages on time (number of MC steps). At the same time, the propagation of oxygen waves on the Pd(110)-(1×2) surface is substantially anisotropic and the elliptic shape of the waves depends on M_x/M_y. As M_x/M_y is increased, the propagating oxygen wave on the surface "elongates" in the $[1\bar{1}0]$ direction. The CO_{ads} diffusion anisotropy effect is still more pronounced in the simulation of spiral oxygen waves on the Pd(110) surface. The simulation of

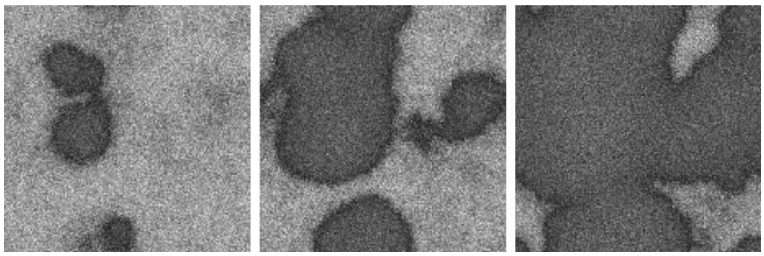

Fig. 5. Distribution of adsorbed substances on the model surface Pd(110) during an increase in the O_{ads} coverage. The dark gray areas are propagating oxygen islands, and the light gray areas are CO_{ads}. The grid size is N =1000. The CO_{ads} diffusion rate parameter is M = 100.

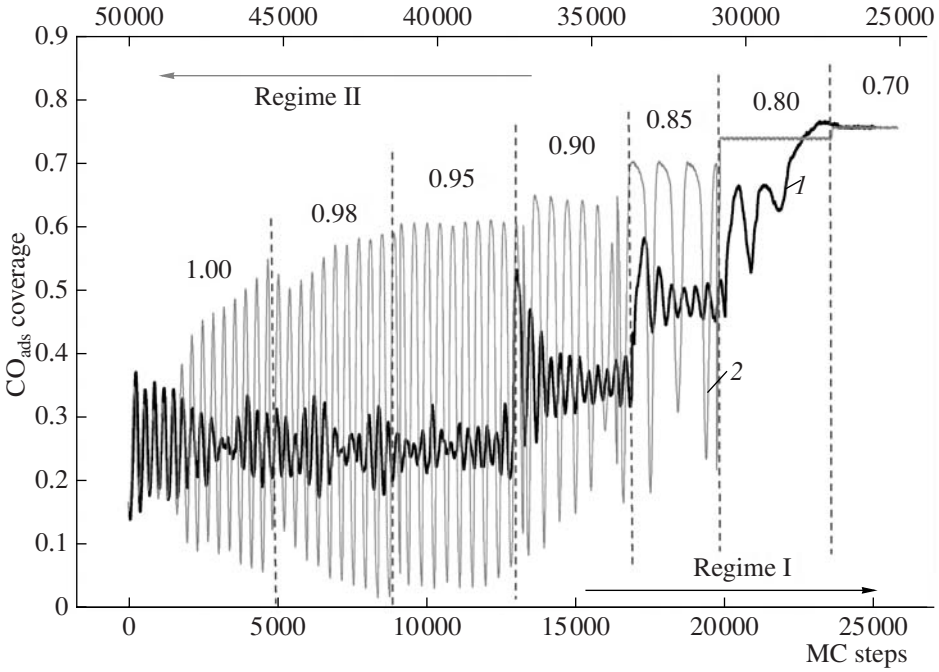

Fig. 6. Characteristics of the two different oscillation regimes resulting from decreasing the rate constant k_1 from 1.0 to 0.7 in steps (regime I, curve *1*) and from raising k_1 from 0.8 to 1.0 (regime II, curve *2*). Only the oscillations of the CO_{ads} coverage are shown. N = 1000; M = 20.

this kind of spatiotemporal structure is detailed in [60]. In our computational experiment, the isotropic diffusion regime (M_x/M_y = 50/50) was changed to an anisotropic diffusion regime with M_x/M_y = 80/20. This led to the "elongation" of the spiral oxygen wave along the $[1\bar{1}0]$ direction [20–22, 61]. This asymmetric behavior is in good agreement with the experimental observation of spiral waves in this reaction by the PEEM method [64].

A numerical study of the CO oxidation dynamics on Pd(110) at a low CO_{ads} diffusion rate (M = 20) gave somewhat unexpected results [62, 63]. As in the case of Pt(100), passing to this M value made the oscillation period and amplitude smaller and irregular. However, as the oxygen adsorption rate constant k_1 (or the oxygen partial pressure P_{O_2}, since $k_1 = k_{ads}(O_2)s_{O_2}P_{O_2}$) was decreased and then increased step-by-step, we observed a hysteresis in the oscillatory behavior of the reaction (Fig. 6), contrary to what was observed for Pt(100). The two oscillation regimes exist at the same k_1 values. They are very different in terms of the oscillation period and amplitude and, moreover, produce different spatiotemporal patterns on the model surface. Which of the regimes will take place depends on the kinetic history of the system. We observed a wide variety of spatiotemporal surface patterns, including cellular and turbulent structures and oxygen waves in the shape of a spiral, ring, or strip. In particular, at the lower boundary of regime I (k_1 = 0.72 s^{-1}), the oxygen waves, which continuously travel over the surface, appear as narrow and long strips. At the lower boundary of regime II (k_1 =

0.83 s^{-1}), the oxygen waves propagate as narrow ring-shaped structures (target patterns).

CONCLUSIONS

The chemical waves on single crystal and tip surfaces result from the interplay among adsorption, reaction, diffusion, and surface reconstruction. Using the kinetic Monte Carlo method, we have investigated the spatiotemporal dynamics of CO oxidation on Pt(100) and Pd(110) single crystal surfaces. The kinetic models for these surfaces differ in the detailed mechanism of the appearance of oscillations. Both models indicate oscillations of the CO_2 formation rate and adsorbed species concentrations. The oscillations are accompanied by wave phenomena on the model surface. We studied the effects of the grid size and CO_{ads} diffusion rate on the synchronization of local processes on the surface and on the oscillation and surface structure patterns. It was deduced that there is a narrow reaction zone when an oxygen wave propagates over the surface, and this was confirmed by APFIM data. Taking into account the longitudinal symmetry of the Pd(110) single crystal has no effect on the oscillation period and amplitude, but leads to elliptic oxygen patterns on the surface. The formation of these patterns is confirmed by surface space-resolved methods (e.g., PEEM). A wide variety of chemical waves (cellular and turbulent patterns, spirals, rings, and strips) can be obtained by varying the parameters of the computational experiment. All of these patterns were actually observed in experimental studies of the oscillatory dynamics of catalytic reactions. In our opinion, the above results make a contribution to the new approaches to developing the theory of heterogeneous catalysis by metals.

ACKNOWLEDGMENTS

This study was supported by the Russian Foundation for Basic Research (grant no. 08-03-00454).

REFERENCES

1. Sheintuch, M. and Schmitz, R.A., *Catal. Rev. Sci. Eng.*, 1977, vol. 15, p. 107.
2. Slinko, M.G. and Slinko, M.M., *Catal. Rev. Sci. Eng.*, 1978, vol. 17, p. 119.
3. Razon, L.F. and Schmitz, R.A., *Catal. Rev. Sci. Eng.*, 1986, vol. 28, p. 89.
4. Ertl, G., *Adv. Catal.*, 1990, vol. 37, p. 213.
5. Yablonskii, G.S., Bykov, V.I., Gorban', A.N., and Elokhin, V.I., in *Kinetic Models of Catalytic Reactions*, Comprehensive Chemical Kinetics, vol. 32, Compton, R.G., Ed., Amsterdam: Elsevier,1991, chs. 5, 6.
6. Imbihl, R., *Prog. Surf. Sci.*, 1993, vol. 44, p. 185.
7. Schüth, F., Henry, B.E., and Schmidt, L.D., *Adv. Catal.,* 1993, vol. 39, p. 51.
8. Eiswirth, M., in *Chaos in Chemistry and Biochemistry*, Fields, R.J. and Györgi, L., Eds., Singapore: World Scientific, 1993, ch. 6, p. 141.
9. Eiswirth, M. and Ertl, G., in *Chemical Waves and Patterns*, Understanding Chemical Reactivity, vol. 10, Kapral, R. and Showalter, K., Eds., Dordrecht: Kluwer, 1994, p. 447.
10. Slinko, M.M. and Jaeger, N.I., *Oscillating Heterogeneous Catalytic Systems*, Studies in Surface Science and Catalysis, vol. 86, Delmon, B. and Yates, J.T., Eds., Amsterdam: Elsevier, 1994.
11. Imbihl, R. and Ertl, G., *Chem. Rev.*, 1995, vol. 95, p. 697.
12. Nieuwenhuys, B.E., *Adv. Catal.*, 1999, vol. 44, p. 259.
13. Ertl, G., *Adv. Catal.*, 2000, vol. 45, p. 1.
14. Cobden, P.D., Janssen, N.M.H., van Breugel, Y., and Nieuwenhuys, B.E., *Faraday Discuss.*, 1996, vol. 105, p. 57.
15. Appendix: Oscillatory Heterogeneous Catalytic Systems, *Catal. Today*, 2005, vol. 105, p. I.
16. Temel, B., Meskine, H., Reuter, K., Scheffler, M., and Metiu, H., *J. Chem. Phys.*, 2007, vol. 126, p. 204711.
17. Fichthorn, K.A. and Weinberg, W.H., *J. Chem. Phys.*, 1991, vol. 95, p. 1090.
18. Zhdanov, V.P., *Surf. Sci. Rep.*, 2002, vol. 45, p. 231.
19. Latkin, E.I., Elokhin, V.I., and Gorodetskii, V.V., *J. Mol. Catal. A: Chem.*, 2001, vol. 166, no. 1, p. 23.
20. Elokhin, V.I., Latkin, E.I., Matveev, A.V., and Gorodetskii, V.V., *Kinet. Katal.*, 2003, vol. 44, no. 5, p. 755 [*Kinet. Catal.* (Engl. Transl.), vol. 44, no. 5, p. 692].
21. Elokhin, V.I. and Gorodetskii, V.V., in *Finely Dispersed Particles: Micro-, Nano-, and Atto-Engineering*, Surfactant Science Series, vol. 130, Spasic, A.M. and Hsu, J.-P., Eds., New York: Taylor & Francis, 2005, ch. 7, p. 159.
22. Gorodetskii, V.V., Elokhin, V.I., Bakker, J.W., and Nieuwenhuys, B.E., *Catal. Today*, 2005, vol. 105, p. 183.
23. Ertl, G., Norton, P.R., and Rustig, J., *Phys. Rev. Lett.*, 1982, vol. 42, p. 177.
24. Thiel, P.A., Behm, R.J., Norton, P.R., and Ertl, G., *Surf. Sci.*, 1982, vol. 121, p. L553.
25. Cox, M.P., Ertl, G., Imbihl, R., and Rustig, J., *Surf. Sci.*, 1983, vol. 134, p. L517.
26. Eiswirth, M., Schwankner, R., and Ertl, G., *Z. Phys. Chem.*, 1985, vol. 144, p. 59.
27. Imbihl, R., Cox, M.P., Ertl, G., Müller, H., and Brenig, W., *J. Chem. Phys.,* 1985, vol. 83, p. 1578.
28. Gorodetskii, V., Block, J.H., Drachsel, W., and Ehsasi, M., *Appl. Surf. Sci.*, 1993, vol. 67, p. 198.
29. Gorodetskii, V., Drachsel, W., and Block, J.H., *Catal. Lett.*, 1993, vol. 19, p. 223.
30. Hopkinson, A., Guo, X.-C., Bradley, J.M., and King, D.A., *J. Chem. Phys.*, 1993, vol. 99, p. 8262.
31. Gorodetskii, V., Drachsel, W., and Block, J.H., *J. Chem. Phys.*, 1994, vol. 100, p. 6907.
32. Gorodetskii, V., Drachsel, W., Ehsasi, M., and Block, J.H., *J. Chem. Phys.*, 1994, vol. 100, p. 6915.
33. Lim, Y.-S., Berdau, M., Naschitzki, M., Ehsasi, M., and Block, J.H., *J. Catal.*, 1994, vol. 149, p. 292.
34. Gorodetskii, V., Lauterbach, J., Rotermund, H.-H., Block, J.H., and Ertl, G., *Nature*, 1994, vol. 370, p. 276.

35. Gruyters, M., Ali, T., and King, D.A., *J. Phys. Chem.*, 1996, vol. 100, p. 14417.
36. Imbihl, R., Cox, M.P., and Ertl, G., *J. Chem. Phys.*, 1986, vol. 84, p. 3519.
37. Drachsel, W., Wesseling, C., and Gorodetskii, V., *J. Phys. IV*, 1996, vol. 6, p. 31.
38. Gorodetskii, V.V. and Drachsel, W., *Appl. Catal., A*, 1999, vol. 188, p. 267.
39. Rotermund, H.H., *Phys. Scr.*, 1993, vol. 49, p. 549.
40. Lauterbach, J., Bonilla, G., and Pletcher, T.D., *Chem. Eng. Sci.*, 1999, vol. 54, p. 4501–4512.
41. Ertl, G. and Rau, P., *Surf. Sci.*, 1969, vol. 15, p. 443.
42. Conrad, H., Ertl, G., Koch, J., and Latta, E.E., *Surf. Sci.*, 1974, vol. 43, p. 462.
43. Matsushima, T. and White, J.M., *Surf. Sci.*, 1977, vol. 67, p. 122.
44. Engel, T. and Ertl, G., *Adv. Catal.*, 1979, vol. 28, p. 1.
45. He, J.-W. and Norton, P.R., *Surf. Sci.*, 1988, vol. 204, p. 26.
46. Ehsasi, M., Seidel, C., Ruppender, H., Drachsel, W., Block, J.H., and Christmann, K., *Surf. Sci.*, 1989, vol. 210, p. L198.
47. Jones, I.Z., Bennett, R.A., and Bowker, M., *Surf. Sci.*, 1999, vol. 439, p. 235.
48. Cobden, P.D., Nieuwenhuys, B.E., and Gorodetskii, V.V., *Appl. Catal., A*, 1999, vol. 188, p. 69.
49. Gorodetskii, V.V., Matveev, A.V., Cobden, P.D., and Nieuwenhuys, B.E., *J. Mol. Catal. A: Chem.*, 2000, vol. 158, p. 155.
50. Gorodetskii, V.V., Matveev, A.V., Kalinkin, A.V., and Nieuwenhuys, B.E., *Chem. Sustainable Dev.*, 2003, vol. 11, p. 67.
51. Gorodetskii, V.V., Matveev, A.V., Podgornov, E.A., and Zaera, F., *Top. Catal.*, 2005, vol. 32, p. 17.
52. Sales, B.S., Turner, J.B., and Maple, M.B., *Surf. Sci.*, 1982, vol. 114, p. 381.
53. Turner, J.B., Sales, B.S., and Maple, M.B., *Surf. Sci.*, 1981, vol. 103, p. 54.
54. Turner, J.B., Sales, B.S., and Maple, M.B., *Surf. Sci.*, 1981, vol. 109, p. 591.
55. Sales, B.S., Turner, J.B., and Maple, M.B., *Surf. Sci.*, 1981, vol. 112, p. 272.
56. Latkin, E.I., Elokhin, V.I., Matveev, A.V., and Gorodetskii, V.V., *J. Mol. Catal. A: Chem.*, 2000, vol. 158, p. 161.
57. Vishnevskii, A.L., Latkin, E.I., and Elokhin, V.I., *Surf. Rev. Lett.*, 1995, vol. 2, p. 459.
58. Elokhin, V.I. and Latkin, E.I., *Dokl. Akad. Nauk*, 1995, vol. 344, p. 56.
59. Elokhin, V.I., Myshlyavtsev, A.V., Latkin, E.I., Resnyanskii, E.D., Sheinin, D.E., and Bal'zhinimaev, B.S., *Kinet. Katal.*, 1998, vol. 39, no. 2, p. 264 [*Kinet. Catal.* (Engl. Transl.), vol. 39, no. 2, p. 246].
60. Latkin, E.I., Elokhin, V.I., and Gorodetskii, V.V., *Chem. Eng. J.*, 2003, vol. 91, p. 123.
61. Matveev, A.V., Latkin, E.I., Elokhin, V.I., and Gorodetskii, V.V., *Chem. Sustainable Dev.*, 2003, vol. 11, p. 173.
62. Matveev, A.V., Latkin, E.I., Elokhin, V.I., and Gorodetskii, V.V., *Chem. Eng. J.*, 2005, vol. 107, p. 181.
63. Elokhin, V., Matveev, A., Gorodetskii, V., and Latkin, E., in *Lecture Notes in Computer Science*, Berlin: Springer, 2007, vol. 4671, p. 401.
64. Block, J.H., Ehsasi, M., Gorodetskii, V., Karpowicz, A., and Berdau, M., in *New Aspects of Spillover Effect in Catalysis*, Studies in Surface Science and Catalysis, vol. 77, Inui, T., Ed., Amsterdam: Elsevier, 1993, p. 189.